Carbohydrate Polymers 192 (2018) 84–94

Contents lists available at ScienceDirect

Carbohydrate Polymers

journal homepage: www.elsevier.com/locate/carbpol

Polyelectrolyte complex of *Aloe vera*, chitosan, and alginate produced fibroblast and lymphocyte viabilities and migration

Raquel Gallardo-Rivera[a], María de los Ángeles Aguilar-Santamaría[a], Phaedra Silva-Bermúdez[b], Julieta García-López[b], Alberto Tecante[c], Cristina Velasquillo[b], Angélica Román-Guerrero[a], César Pérez-Alonso[d], Humberto Vázquez-Torres[e], Keiko Shirai[a,*]

[a] *Universidad Autonoma Metropolitana, Biotechnology Department, Laboratory of Biopolymers and Pilot Plant of Bioprocessing of Agro-Industrial and Food By-Products, Av. San Rafael Atlixco No. 186, Iztapalapa 09340, Mexico City, Mexico*
[b] *Instituto Nacional de Rehabilitacion, Mexico City, Mexico*
[c] *Universidad Nacional Autonoma de Mexico, Food and Biotechnology Department, Faculty of Chemistry, Mexico City, Mexico*
[d] *Universidad Autonoma del Estado de Mexico, Faculty of Chemistry, State of Mexico, Mexico*
[e] *Universidad Autonoma Metropolitana-Iztapalapa, Physics Department, Av. San Rafael Atlixco, No. 186, 09340, Mexico City, Mexico*

ARTICLE INFO

Chemical compounds used in this article:
Chitosan (PubChem CID:71853)
Sodium alginate (PubChem CID: 91666323)
Calcofluor white (PubChem CID: 6108780)
Calcein-AM (PubChem CID:4126474)
Ethidium homodimer (PubChem CID: 12328897)
(3-(4,5-Dimethyl-thiazol-2-yl)-2-5-diphenyltetrazolium bromide (PubChem CID: 64965)
Dimethyl sulfoxide (PubChem CID: 679)
Isopropyl alcohol (PubChem CID: 3776)

Keywords:
Aloe vera
Chitosan
Lymphocyte
Fibroblast
Cell viability
Polyelectrolyte complex

ABSTRACT

Chitosan, sodium alginate and gel of *Aloe vera* (*Aloe barbadensis* Miller) were employed for the preparation of polyelectrolyte complexes at pH 4 and 6. FT-IR spectroscopy analysis showed evidence on complexes formation and incorporation of the *Aloe vera* gel. The ζ potential determination of the polyelectrolyte complexes revealed the presence of surface charges in the range of −20 to −24 mV, which results in stable systems. The dynamic moduli exhibited a high dependence on angular frequency, which is commonly found in solutions of macromolecules. The materials showed human fibroblast and lymphocyte viabilities up to 90% in agreement with null cytotoxicity. The polyelectrolyte complexes at pH 6 with Ca^{2+} were stable, showed high water absorption, satisfactory morphology, pore size and rigidity, characteristics that allowed significant human fibroblast migration in wound closure *in vitro* assays.

1. Introduction

Chitosan (CH) is a cationic polysaccharide with mucoadhesive, hemostatic and antimicrobial properties. Additionally, CH enhances wound healing due to stimulation of fibroblast proliferation and production of type III collagen (Panneerselvam, Merlin, Kalaivani, Baran, & Rose, 2013).

The use of CH and alginate (ALG) macromolecular networks are reported for several biomedical applications such as encapsulation, incorporation, and release of cells, drugs, and therapeutic agents (Lawrie et al., 2007; Simó, Fernández-Fernández, Vila-Crespo, Ruipérez, & Rodríguez-Nogales, 2017). Another natural component that has attracted increasing interest is the *Aloe vera* (*Aloe barbadensis* Miller) gel (AV), which has been claimed as a wound healer, immunomodulatory and anti-inflammatory, as well as a promoter of growth of epithelial tissue and activator of macrophage (Hamman, 2008). The biological activities of AV are mainly related to acemannan (AC), which is composed of a long chain of acetylated mannose with glucose and galactose residues (Simões, Nunes, Domingues, Coimbra, & Domingues, 2012).

Blends of CH and AC gels have been reported by Escobedo-Lozano, Domard, Velázquez, Goycoolea, and Argüelles-Monal (2015) to study their mechanical, thermal and antibacterial properties. Other reports include the production of membranes of AV and CH to study the

* Corresponding author.
E-mail address: smk@xanum.uam.mx (K. Shirai).

https://doi.org/10.1016/j.carbpol.2018.03.044
Received 1 August 2017; Received in revised form 14 March 2018; Accepted 16 March 2018
Available online 19 March 2018
0144-8617/

adherence of L929 fibroblast-like cells (Silva, Caridade, Mano, and Reis (2013), as well AV/CH/vitamin E microparticles produced by spray drying for a second-degree burn mouse model (Garrastazu-Pereira et al., 2014) or the production of 3D porous scaffold architectures of CH and AV combined with collagen (Panneerselvam et al., 2013). Noteworthy, the important features of these materials are highly dependent on AV concentration such as the water absorption capacity, hydrophilicity and *in vitro* enzymatic degradation as suggested by Pereira, Carvalho, Gil, Mendes, and Bártolo (2013) in their work in AV-Ca-ALG hydrogel films with several AV contents.

Nonetheless, despite of these reports on CH and AV, there is a lack of information on the role of AV in the material formation, physicochemical and biological properties, and also in the characterization that is an essential issue for application as might vary depending on the batch. Moreover, there is no information, to the best of our knowledge, on the incorporation of AV in PECs based on CH and ALG, nor the effect of pH and Ca^{2+} on human dermal fibroblasts (HDF) migration and viability of lymphocytes (HL) and HDF. Therefore, the aim of this study was to prepare PECs by ionic interaction between CH, ALG, and AV, which were fully characterized and studied *in vitro* with human cells, fibroblasts and lymphocytes.

2. Materials and methods

2.1. Materials

Commercial chitosan (QCH), sodium alginate (ALG) and calcofluor white were supplied by Sigma-Aldrich (St Louis MO USA). Another chitosan sample (BCH) was produced from deacetylation of chitin extracted by a biological method (Pacheco et al., 2011). Dulbecco's Modified Eagle Medium (DMEM-F12), fetal bovine serum (FBS), phosphate buffer saline solution (PBS), collagenase type I, dispase II, antibiotic (penicillin/streptomycin), 0.25% trypsin-EDTA and Hank's balanced salt solution were supplied by Gibco (USA). LIVE/DEAD® viability/cytotoxicity kit for mammalian cell (calcein-AM and ethidium homodimer) and fluorescent secondary antibodies Alexa Fluor 594® (A21207) and Alexa Fluor 488® (A11001) were purchased from Molecular Probes, Invitrogen (USA). Primary antibodies anti-Collagen Type I (ab6308), anti-tropoelastin (ab21600) and anti-fibroblasts surface protein (ab11333) were acquired form Abcam plc (USA). 3-(4,5-dimethyl-thiazol-2-yl)-2-5-diphenyltetrazolium bromide (MTT) (M2128, 10 mg/mL aliquots), dimethyl sulfoxide (D2650), 4′,6-Diamidino-2-phenylindole dihydrochloride (DAPI) and HPLC grade glucose, mannose, galactose, fructose were supplied by Sigma-Aldrich (USA). Isopropyl alcohol was supplied by J.T. Baker (Mexico).

2.2. CH and ALG characterization

Degree of acetylation (DA) of CH was determined by proton nuclear magnetic resonance (^{1}H NMR) spectroscopy in a Bruker (Advance III 500, Germany) at 200 MHz using 3-(trimethylsilyl) propionic acid as the internal reference. Powder X-ray diffraction (PXRD) spectra were acquired in a Bruker D-8 Advance diffractometer (Germany) in air at room temperature (25 °C) with one-dimensional positive silicon detector (Bruker Lynxeye, Germany). Diffraction intensity as a function of 2θ angles was measured between 5 and 70°, with a 2θ step of 0.02037° and 0.4 s per point. Percentage of crystallinity was calculated according to Abduo, Nagy, and Elsabee (2008). Viscosity average molecular weight (M_v) for CHs were determined from their intrinsic viscosities using 0.25 M acetic acid/0.25 M sodium acetate solution and measured with Ubbelohde capillary viscometer according to Pacheco et al. (2011). Apparent viscosity of ALG 2 wt% aqueous solution was determined at 20 rpm and at 20 °C in a Brookfield DVI viscometer (Brookfield Engineering Middleborough, MA USA).

2.3. AV and AC extraction and characterization

AV was prepared from the inner part of three-year-old plants collected in 2014 from a plantation in the city of Toluca (Mexico). Fresh leaves of 28 cm in average length were washed with distilled water. Plant skin was separated from the parenchymal tissue as described by Silva, Popa et al. (2013). The gel was washed with deionized water to remove the exudates from its surfaces. Then, cut into small cubes and placed in a glass container for homogenization with a hand blender (Phillips, USA), filtered (40 μm) and stored at 3 °C (± 1 °C) until use. AC was extracted from AV (10 mL) by precipitation in ethanol (anhydrous) (30 mL) at 8 °C during 24 h, followed by centrifugation at 1126 rpm in a Thermo Fisher Sorvall Legend XT/XF (Waltham MA, USA) for 15 min at 4 °C. The pellet was mixed in deionized water and stirred with mechanical agitation at 8 °C for 24 h. Subsequently, the suspension was filtered (0.45 μm) and lyophilized (Ni, Turner, Yates, & Tizard, 2004).

Viscoelastic properties of the AV were determined at 25 °C using amplitude oscillatory shear (SAOS) tests in a ARES-RFS III TA-Instruments rheometer (New Castle DE, USA) with grooved parallel plates of 25 mm diameter and 1.00, 1.60 and 1.65 mm gaps. Strain sweeps (0.1-100% strain) were performed at a constant angular frequency (1 Hz) to determine the extension of the linear viscoelasticity zone (ZLV). A strain of 1% was chosen to perform frequency sweeps at 0.1–100 rad/s. Storage modulus (G'), and the loss modulus (G") were recorded as a function of frequency.

Concentrations of free sugars fructose, glucose, mannose and galactose in AV gel were determined by liquid chromatography by in an Agilent 1260 infinity (Santa Clara, CA, USA) HPLC equipped with an autosampler, a refractive index detector and a SHODEX Asahipak NH_2P-50 (4.6 mm × 250 mm) column (Showa Denko Tokyo, Japan) with acetonitrile/water (75:25) mobile phase in 0.6 mL/min flow at 25 °C (Bozzi, Perrin, Austin, & Arce Vera, 2007). AV and AC (10 mg) were dissolved in deuterium oxide (0.7 mL), and the degree of acetylation (DA) was determined by ^{1}H NMR (Chokboribal et al., 2015).

2.4. Determination of polyelectrolyte complex (PEC) composition

ALG was hydrated with deionized water during 1 h and added to a CH solution in acetic acid (0.1 M). In a typical procedure, the AV was added to the CH/ALG solution and mixed in vortex for 30 s. Then, the blend was homogenized with an Ultra-Turrax (IKA Staufen, Germany) at 7000 rpm for 1 min. pH was adjusted at 4 or 6 by the addition of NaOH (1 N) and sonicated (Branson, Danbury CT, USA) for 10 min to eliminate air bubbles and stored at 3 °C prior to use.

Weight ratios in PECs were AV = 30 vol% (0.345 wt%), 2, 2.5, 3 wt % for CH and 0.5, 1 and 2 wt% for ALG. Average pore size diameter (APS) was determined by scanning electron microscopy (SEM) using ImageJ software with a minimum of 20 determinations for each sample (Schneider, Rasband, & Eliceiri, 2012). Black areas in the micrographs represent the pores, and white areas assigned to solid surfaces. PECs were prepared with QCH or BCH (2%), ALG (2%) and AV (30%) at a weight ratio of 0.46:0.46:0.08 and adjusting at pH 4 and 6, CQCH-4, CBCH-4, CQCH-6, and CBCH-6. $CaCl_2$ (1 mM) was added to PECs prepared at pH 6 to give CQCH-6-Ca and CBCH-6-Ca. CH-ALG complexes (2 wt%) were also produced at pH 4 and 6 as control samples and labeled as BQCH-4, BBCH-4, BQCH-6, BBCH-6, BQCH-6-Ca, and BBCH-6-Ca.

2.5. Physicochemical characterization of the PECs

FTIR spectra (4000 to 650 cm^{-1}) of freeze-dried PEC samples were acquired in a Perkin Elmer 100 spectrometer (Waltham MA, USA) with attenuated total reflectance Fourier transform infrared (ATR-FTIR) as the average of 32 scans and at a resolution of 4 cm^{-1}. Each component was also lyophilized and mixed at the same concentration than the PEC

as control samples without ionic interactions and analyzed by FTIR. ζ potentials of 1 wt% ALG, 0.1 wt% AV, 0.5 vol% CH, as well as 0.7 wt% CQCH-4, CBCH-4, CQCH-6 and CBCH-6 in 0.3 M acetic acid/0.2 M sodium acetate solution were measured using a Zetasizer Nano Series instrument (Malvern Instruments Worcestershire, UK). Viscoelastic properties of PECs were determined using the conditions explained in Section 2.3. Dried materials (5 mg) were suspended in 3 mL of phosphate buffer (pH 7.2) with 10 μL of calcofluor white-reagent (CWR) and vortexed for 20 s. After 2 h of reaction, samples were centrifuged at 5000 rpm for 10 min and pellet was observed in a microscope with fluorescent light (Carl Zeiss, Germany) and analyzed by ImageJ software (Zhang et al., 2015). SEM analyses were performed in a JSM-7600F SE microscope (Jeol Co. Ltd., Tokyo, Japan) with low magnification mode and at 15 kV accelerating voltage with samples mounted on carbon sample holders sputtered with gold in high vacuum (Denton Vacuum DESK IV Moorestown NJ, USA). Swelling capacities and weight loss determinations for PECs were conducted by immersion in DMEM-F12 (5 mL) containing 0.1 g of dry sample at 37 °C and monitored during 24 h. Swollen sample weights were measured after removing the excess of surface water with filter paper. Percentage of swelling capacity (S) at equilibrium was determined by Eq. (1).

$$S = \left(\frac{(w - w_0)}{w_0}\right) \times 100 \quad (1)$$

where w is the sample weight, and w_0 is the initial dry weight.

Weight loss (WL) was calculated from the initial dry weight (w_0) and the final dry weight (w_f) subtracting the weight of DMEM-F12 salts (w_{salts} = 5.34 mg/mL) by Eq. (2).

$$WL = \left(\frac{(w_0 - (w_f - w_{salts}))}{w_0}\right) \times 100 \quad (2)$$

2.6. HDF and HL viabilities

HDFs were isolated from foreskin biopsies of pediatric patients with parental informed consent and the process was approved by the Institutional Committee on Human Research of the Instituto Nacional de Rehabilitacion Luis Guillermo Ibarra Ibarra (Mexico) (Project registry INR-1112). Foreskin biopsies were washed in penicillin-streptomycin 10 vol% solution in PBS (1X PBS, pH = 7.4), adipose tissue was removed and the dermis was separated from the epidermis using dispase II. Then, epidermis was discarded and dermis was digested in collagenase Type I to isolate the HDFs. Cells were seeded in culture flasks and cultured with DMEM-F12 supplemented with 10 vol% FBS and 1vol% penicillin-streptomycin. Culture medium was changed every two days until 80% cell confluence. Cultures were incubated at 37 °C, 80% relative humidity and 5% of CO_2 unless stated otherwise. 80% confluent cells were rinsed with PBS and treated with 0.05% trypsin-EDTA to collect them from flasks. Cell pellet was collected after centrifugation, suspended in supplemented DMEM-F12 and seeded in culture flasks for cell expansion until passage 3–4, when HDFs were used for viability and wound closure (scratch) assays. Expanded HDFs were recollected, centrifuged, seeded in 24-well culture plates at a 1.8×10^4 cells/cm^2 and cultured with supplemented DMEM-F12 at 37 °C and 5% CO_2 atmosphere until 90% cell confluence. Then, cell culture medium was removed and 2.0 mL of PEC:supplemented DMEM-F12 solution at a ratio of 1:1.5 (v:v) was added. Samples were cultured and cell viability was assessed at 24 h. PECs were used as gels and sterilized by ultraviolet radiation (λ = 254 nm) for 40 min before the addition to culture wells. Positive control samples corresponded to HDF cultured with a mixture of DMEM-F12:supplemented DMEM-F12 in a 1:1.5 volume ratio for all *in vitro* experiments. Cell viability in 24 h culture was assessed qualitatively using the LIVE/DEAD® Viability/Cytotoxicity kit; samples were rinsed with PBS and calcein-AM/ethidium homodimer was added according and incubated for 40 min at 37 °C. Samples were rinsed with PBS and observed in the microscope (Axio Observer Carl Zeiss). Images were processed using the AxioVision© software. Cell viability was assessed quantitatively by evaluation of cell metabolic activity using MTT reagent. Samples of HDFs cultured overnight in PEC:supplemented DMEM-F12 were rinsed twice with PBS, and MTT solution (0.5 mg/mL) was added. HDFs were incubated for 4 h. Later on, DMSO: isopropyl alcohol 1:1 solution was added and the absorbance of colored formazan crystals dissolution was measured at 540 nm with a plate reader (DTX 800 Multimode Detector, Beckman Culture). Cell growth (X) was calculated according to Eq. (3).

$$X = \left(\frac{OD_s}{OD_b}\right) \times 100 \quad (3)$$

where OD_s is the optical density of sample and OD_b is the optical density of the blank (cells cultured with DMEM-F12:supplemented-DMEM-F12 solution without PEC).

Fibroblastic phenotype of isolated HDFs was corroborated by cell morphologies upon culture and immunofluorescence assays against fibroblasts surface protein antibody, collagen Type I and elastin as previously reported by Velasquillo et al. (2017). Briefly, cells in passage 3–4 were seeded in 48-well culture plates (in addition to cells seeded in 24-well culture plates for PECs studies), cultured for 7 days, fixed with PFA (2 vol%), permeabilized with 0.3 wt% triton, blocked with 1 wt% albumin and independently incubated overnight with primary antibodies against either collagen Type I (ab6308; 1:500), tropoelastin (ab21600; 1:100) or fibroblasts surface protein (ab11333; 2:100). Primary antibodies were removed and samples were incubated at 37 °C with Alexa Fluor 594® (A21207; 1:300) or Alexa Fluor 488® (A11001; 1:300). Cells nuclei were counterstained with DAPI. Finally, samples were washed and examined by microscopy.

For the HL viability determination, blood samples from seven consent 26 years-old average age healthy donors were taken using heparinized syringes. 0.5 mL of whole blood was added to Nunc tubes that contained 2.5 mL of 5a Modified McCoy medium with 4 wt% of phytohaemaglutinin and 0.4 wt% antibiotic solutions (penicillin-streptomycin). The addition of phytohaemaglutinin to HL culture agglutinates erythrocytes and leucocytes, as well as stimulates lymphocytes (Dao-Thi et al., 1996). Cultures were incubated for 24 h. Then, transferred to Petri dishes (5 cm diameter) containing the sterilized PECs and incubated for 48 h. Cells were re-suspended in PBS and centrifuged at 1500 rpm for 10 min. A 75 μL aliquot of the buffy coat was transferred to another tube and incubated with erythrocyte lysis buffer for 15 min. Microscopic observations corroborated the HL morphologies at 24 and 48 h of culture. HLs pellets were treated as previously described for MTT assay and neutral red (NR) assay (Repetto, Del Peso, & Zurita, 2008). HL viability with MTT and NR assays were calculated according to Eq. (3).

2.7. Evaluation of HDFs migration

The effect of PECs and their components (CH, ALG and AV) on the HDF migration was assessed by the *in vitro* scratch assay. Expanded HDFs in passage 3–4 were recollected from culture flasks, centrifuged, seeded in 12-well culture plates at a 1.8×10^4 cells/cm^2 and incubated with supplemented DMEM-F12 until 90% cell confluence. To perform the scratch assays, culture medium was removed and scratch was formed on the 90% confluent HDF monolayers using a pipet tip of approximately 900 μm width. Samples were rinsed with supplemented-DMEM-F12 to remove cells debris. CH, ALG, AV or PECs-supplemented DMEM-F12 solutions were added, and samples were incubated overnight. Images of the scratch areas were acquired before and after overnight incubation using a phase contrast microscope (Axiovert 25 Carl Zeiss) and analyzed using the TScratch software (Gebäck, Schulz, Koumoutsakos, & Detmar, 2009).

2.8. Statistical analyses

Experimental data were processed by analysis of variance for balanced data (ANOVA) for two-factor interactions with Tukey-Kramer multiple comparisons of means test ($p \leq 0.05$). Experiments were conducted by triplicate. Results of biological assays were expressed as means and their standard deviation.

3. Results and discussion

3.1. CH, ALG, AV and AC characterization

The viscometric molecular weight and DA of QCH were M_v = 216.4 kDa and DA = 20%, respectively, which were higher than that for BCH (M_v = 140.7 kDa and DA = 9%). Nonetheless, BCH presented greater crystallinity (64%) than QCH (46%) notwithstanding the high DA of QCH. According to the previous work by Pacheco et al. (2011) the chitosan obtained from biological chitin preserved the crystalline structure with relatively large crystallites than that by the chemical process. The XRD pattern of ALG shows a semi-crystalline structure with two diffraction peaks at 2θ = 14.6° and 21.5° with 18% of crystallinity and apparent viscosity of 122 ± 5.6 mPas, corresponding to a low molecular weight ALG.

AV is the leaf parenchyma that contains mostly water (> 98%) and polysaccharides such as, pectins, cellulose, hemicellulose, glucomannan, AC and mannose derivatives (Bozzi et al., 2007). The sugar composition of AV and AC, shown in Table 1, displayed glucose, mannose and galactose contents as the most abundant monosaccharides in both AV and AC. These results are in agreement with previous reports on the characterization of AV and AC (Ni et al., 2004; Bozzi et al., 2007). The signals in the AV ^{1}HNMR spectra at 5.4 ppm, 4.2 ppm and 2-2.4 ppm were assigned to glucose, malic acid, and AC, respectively (see Supplementary data 1) (Bozzi et al., 2007).

The AC content in AV was 19 mg/100 mg of AV in dry basis, which is in the adequate range for isolated AC (at least 10% wt/wt) according to Bozzi et al. (2007). The DA of 38% in AC was higher than the 18% previously reported by Escobedo-Lozano et al. (2015), while DA of AV was 12% (see Supplementary data 1 for ^{1}HNMR spectra of AC and AV). Noteworthy, DA plays a key role in the structure and biological properties; fully deacetylation alters ACs conformation and thereby decreases the bioactivity for induction of cell proliferation and gene expression of vascular endothelial growth factor and Collagen I (Chokboribal et al., 2015).

3.2. Effect of CH and ALG concentration on PECs formation and physicochemical properties

The APS was determined in each PEC formulation varying QCH and ALG concentrations keeping AV at 30% (0.345 wt%) and the results are shown in Supplementary data 2. Generally, finding the best hydrogel microarchitecture toward adequate APS for cell ingrowth, migration, and secretion of extracellular matrix (ECM) in tissue regeneration is challenging. In this regard, optimum pore size for regeneration of adult mammalian skin has been reported in the 20–125 μm range (Annabi et al., 2010). However, best proliferation and ECM production was observed between 250 and 500 μm in genipin-crosslinked gelatin scaffolds (Lien, Ko, & Huang 2009). In the present work, the increment in CH concentration increased the APS, 2% (138 ± 45.4 μm) and 2.5% (97.5 ± 50.2 μm), with significant differences to that with 3% (524.3 ± 50.86 μm). The ALG concentration displayed similar effect, when 0.5% of ALG, the APS was significantly smaller (24.5 ± 45.8 μm) than those at 1% (422.4 ± 41.7 μm) and 2% (249.7 ± 71.7 μm). The statistical analysis shows four groups with significant differences among CH:ALG ratios in 30% AV formulations: i) 2:0.5 (2.82 μm), 2.5:0.5(15.56 μm) and 3:0.50 (42.6 μm); ii) 2:1 (86.9 μm); iii) 2.5:1 (179.3 μm) and 2:2 (249.7 μm); iv) 3:1(1031.3 μm). The PEC formulation group iii presented suitable APS, which was in agreement to Lien et al. (2009) and Annabi et al. (2010). Therefore, 30% AV, 2% CH, and 2% ALG blend was selected for further experimentation.

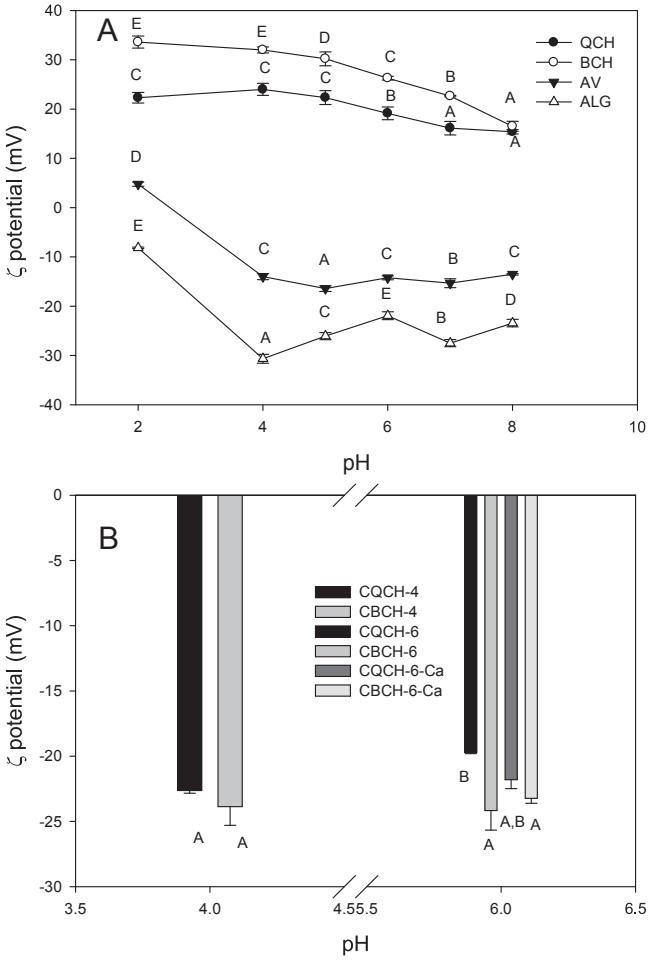

Fig. 1. ζ Potential of polysaccharides (A) and PECs (B) determined at several pH. Different letters in a plot or histogram mean that the groups are significantly different according to multiple comparisons of means Tukey-Kramer test ($p \leq 0.05$).

Table 1
Sugar composition of AV and AC in dry basis.

Sugar content (mg monosaccharide/100 mg)					
	Fructose	Manose	Galactose	Glucose	Total
AV[a]	0.51 ± 0.0002	0.91 ± 0.022	0.77 ± 0.001	2.86 ± 0.027	5.05
AC[b,c]	14.20 ± 0.004	25.35 ± 0.016	16.95 ± 0.013	39.43 ± 0.062	95.92

[a] DA = 12 ± 1% and 11.5 mg AV/ml.
[b] 19 mg AC/100 mg AV.
[c] DA = 38 ± 1.32%.

The ζ potential values of QCH and BCH (Fig. 1) showed a polycationic behavior, although BCH ζ potential was significantly higher than that for QCH. This might be ascribed to the lower content of acetyl groups and, the consequently enhanced amine protonation. For both samples, the ζ potential increased as the medium became acidic, and at neutral pH, the ζ potential of CH was significantly reduced. Contrarily, ALG exhibited a polyanionic behavior in the range of pH 2.0-8.0 owing to dissociation of the carboxylic moiety. The AV displays a polycationic behavior at pH 2 (+4.7 mV) and polyanionic at the 3.0–8.0 pH range (−13 at −16 mV), which substantiates that the particles tend to acquire negative charges at alkaline pH. AV ionic behavior is mainly attributed to pectin, while AC and other components have no ionic charges.

The ζ potential values of PECs prepared at pH 4 and 6 displayed a polyanionic behavior in the −20 to −24 mV range (Fig. 1), indicating components with negative surface charges, ALG and AV. In accordance with the core-shell PEC model proposed for CH-ALG complexes, small non-aggregating particles prevailed in our materials thereby the polyanion might form a stabilizing shell around the particles (Sæther, Holme, Maurstad, Smidrød, & Stokke, 2008). The ζ potential values of PECs prepared with BCH were lower than those with QCH indicating that BCH increased system stability. A plausible explanation for this experimental evidence is the higher DA and M_v of QCH (DA = 20% and M_v = 216.4 kDa) than values for BCH (DA = 9% and M_v = 140.7 kDa). CH molecular weight affects the rate and the extent of binding to ALG beads. According to this, a lower degree of polymerization displays a rapid diffusion into the gel, while CH with higher *M*v only binds to ALG bead surface. Additionally, the presence of acetyl groups significantly decreased the binding among CH and ALG (Gåserød, Smidsrød, & Skjåk-Bræk, 1998), and consequently, the higher DA the smaller the binding between CH and ALG. The formation of PECs prepared at physiological pH (ca. 7.4) was considered for further experimentation on human cell viabilities however, this approach was ruled out because it induced flocculation. The loss in stability due to the less protonated CH, and the remaining protonated groups available for interaction might lead to overall weaker electrostatic interactions at pH 7 (Sæther, Holme, Maurstad, Smidrød, & Stokke, 2008).

On the other hand, FTIR spectra of PECs and its individual components are shown in Fig. 2. For BCH and QCH, the NH_3^+ group displays the stretching vibration band at 3300 cm^{-1} and those of asymmetrical and symmetrical bending at 1600 and 1421 cm^{-1}, respectively. The characteristic band at 1650 cm^{-1} was assigned to the −C═O group of the acetylated fraction of CH, which was more intense for QCH than for BCH concomitantly with the measured DA (Table 1). The AV spectrum shows a band at 3300 cm^{-1} assigned to the −O−H stretching with its bending vibration at 1028 cm^{-1} appointed to glucans. The band at 2923 cm^{-1} corresponds to −C−H stretching, and C═O vibrations observed at 1728 cm^{-1} are due to stretching of the acetyl ester (Chang, Chen, & Feng, 2011). The band at 1589 cm^{-1} is assigned to carboxylate, and C−O− stretching vibration of acetyl ester group at 1241 cm^{-1} and that at 1064 cm^{-1} to mannose according to Kačuráková, Capek, Sasinková, Wellnerb, and Ebringerová (2000). The ALG presents the characteristic functional group −OC═O with a broad band due to the asymmetrical stretching near 1595 cm^{-1} and a narrower band due to the symmetrical stretching at 1406 cm^{-1}. The sharpening of the band at 1598 cm^{-1} in PEC spectra is attributed to the ionic interaction of the carboxylate groups of polyanionic ALG with $-NH_3^+$ groups of polycationic CH (Abreu, Bianchini, Forte, & Kist, 2008). This change might lead to the disappearance of the band at 1728 cm^{-1} of AV in the PECs, possibly as a result of hydrogen bond interactions of AV with CHs, accordingly to the lowest weight ratio of AV in PEC, which is 0.08 while for CH and ALG are of 0.46, respectively. It is worth mentioning that a band at 1240 cm^{-1} assigned to concerted stretching-bend vibrations of −C−OH bond of carboxyl group appeared in FTIR spectra of the mixtures of components (Fig. 2B) but not in PEC spectra.

The broad −OH stretching band at 3300–3050 cm^{-1} substantiates the presence of hydrogen bonding (Fig. 2A and B) which is related to the complex mixture of polysaccharides, such as pectin, cellulose, and AC glycoproteins in AV (Bozzi et al., 2007).

The FTIR-ATR spectra of mixtures of lyophilized components showed bands at 1730 cm^{-1} assigned to the carbonyl group of AV in all the combinations (Fig. 2B). Thus, the disappearance of this band in the PECs from aqueous solution confirms that water allows a close interaction among components, and therefore the formation of hydrogen bonds in agreement with Berger et al. (2004).

3.2.1. Rheological behavior

The shear viscosities of AV, CH, and ALG decreased with an increasing shear rate corresponding to a non-Newtonian fluid with a shear thinning behavior (see Supplementary data 3 Viscosity and dynamic viscoelastic behavior of AV). On the other hand, the extension of the ZLV for PECs showed typical behavior of flowing materials without any gel character from a rheological standpoint; thus, revealing no real crossing of the G' and G" curves (Supplementary data 4 for ZLV of PECs). The variation of dynamic moduli with angular frequency carried out to determine the viscoelastic behavior of the PECs, displayed for all samples an increase with angular frequency, and G" was always greater than G' (Fig. 3). The PECs prepared at pH 4 (Fig. 3A), CQCH-4 and CBCH-4, had similar loss modulus, whereas for complexes prepared at pH 6, G" of CQCH-6 was higher than CBCH-6, which might be associated to the higher DA of QCH than BCH (Table 1). The dynamic moduli were less dependent on the frequency at pH 6 which suggests the presence of increasingly rigid structures. Structure rigidity might be attributed to electrostatic interactions between the amino groups of CH and the acid groups of ALG.

It is important to note that ALG is known to form gels in the presence of divalent cations, e.g. Ca^{2+}, which act as cross-linkers between the functional groups of alginate chains and the carboxyl groups of the polyuronic acid residues, mainly polyguluronic, as depicted by the "egg box" model (Yang, Campanella, Hamaker, Zhang, & Gu, 2013). The G content and the length of the block sequence in the ALG chain contribute to gel-forming ability and gel strength. The presence of Ca^{2+} in G-rich ALG lead to strong but brittle gels while M-rich ALG gels are weak but elastic. Although CBCH-6-Ca and CQCH-6-Ca presented similar values of viscous modulus and G" greater than G' (Fig. 3), dynamic moduli were not congruent at high frequencies as reported Zhang et al. (2015). The concentration of Ca^{2+} ions (1 mM) was not sufficient to form true gels, i.e. gels supporting their weight. However, this concentration of Ca^{2+} was chosen due to human cell compatibility of PECs, in which divalent ions are used at concentrations lower than 1 mM in order to avoid cell metabolic disturbance (Bunse et al., 2013). Additionally, it has been reported that ECM rigidity regulates fibroblast behavior by inducing focal adhesions on soft (400 Pa) and stiff (5000 Pa) cross-linked polyacrylamide gels. HDFs grew significantly better on rigid than soft gels although it adhered similarly in soft and stiff gels. Focal complexes among cells and rigid gels are formed and might contribute to aberrant epithelial tissue behavior by influencing integrin adhesions, which were higher on those with stiff matrix than those with the soft matrix (Paszek et al., 2005). The storage moduli of PECs observed in this study ranged from G' = 0.01 to 100 Pa, which is in the same order of magnitude of the soft cross-linked polyacrylamide gels (400 Pa).

3.3. Morphology of PECs

3.3.1. Fluorescence microscopic analysis

The fluorescence signals of PECs-CWR labeled complex in Fig. 4 evidence the formation of microgels in the system due to the interaction of CWR with 1,4-β−glucans as CH inducing fluorescence. This observation confirms the presence of incipient networks, possibly microgels instead of three-dimensional networks. The microgels have been

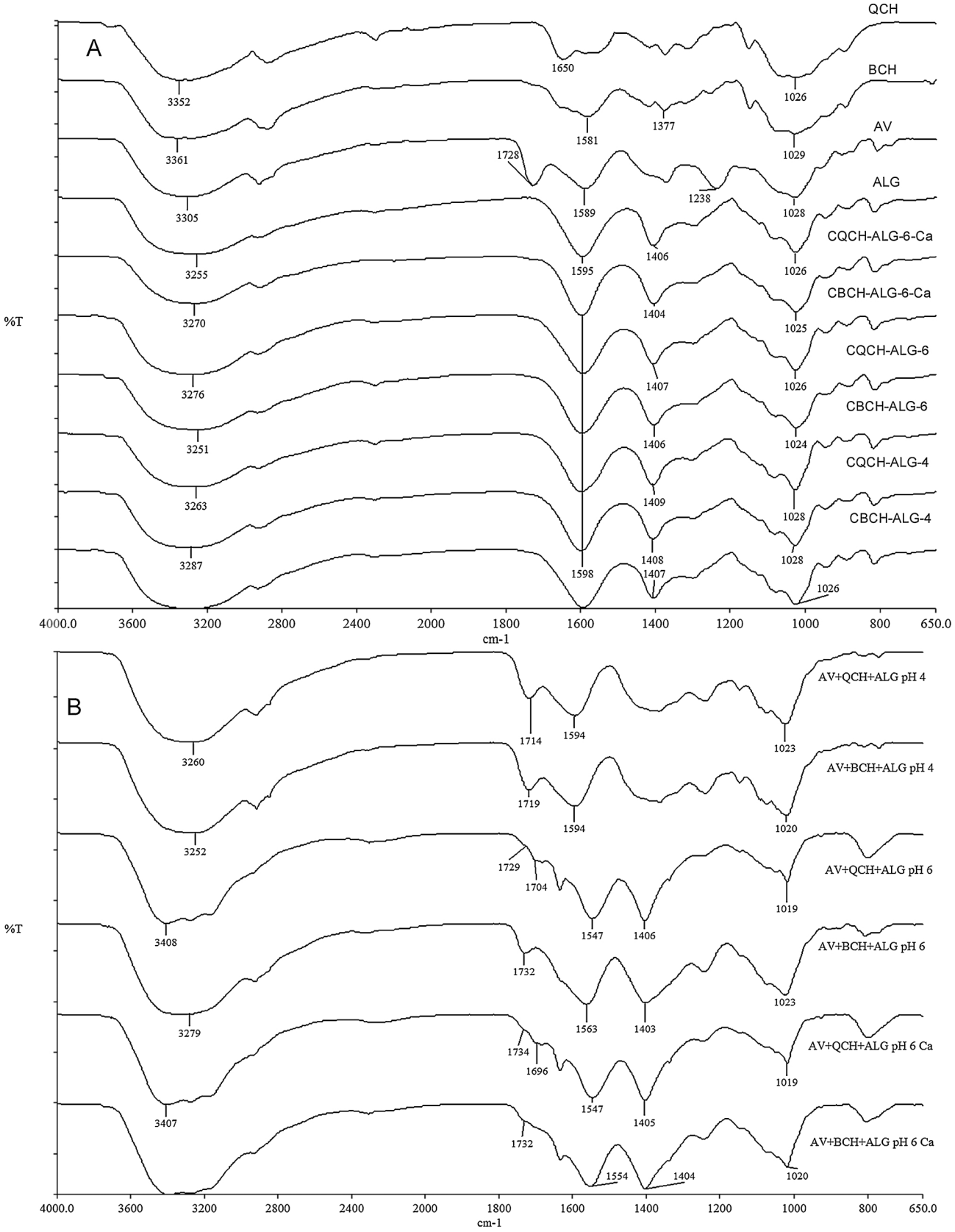

Fig. 2. FTIR-ATR spectra of CH, ALG, AV and PECs at pH 4, pH 6 with and without Ca^{2+} ions (A) and mixtures of lyophilized components (B).

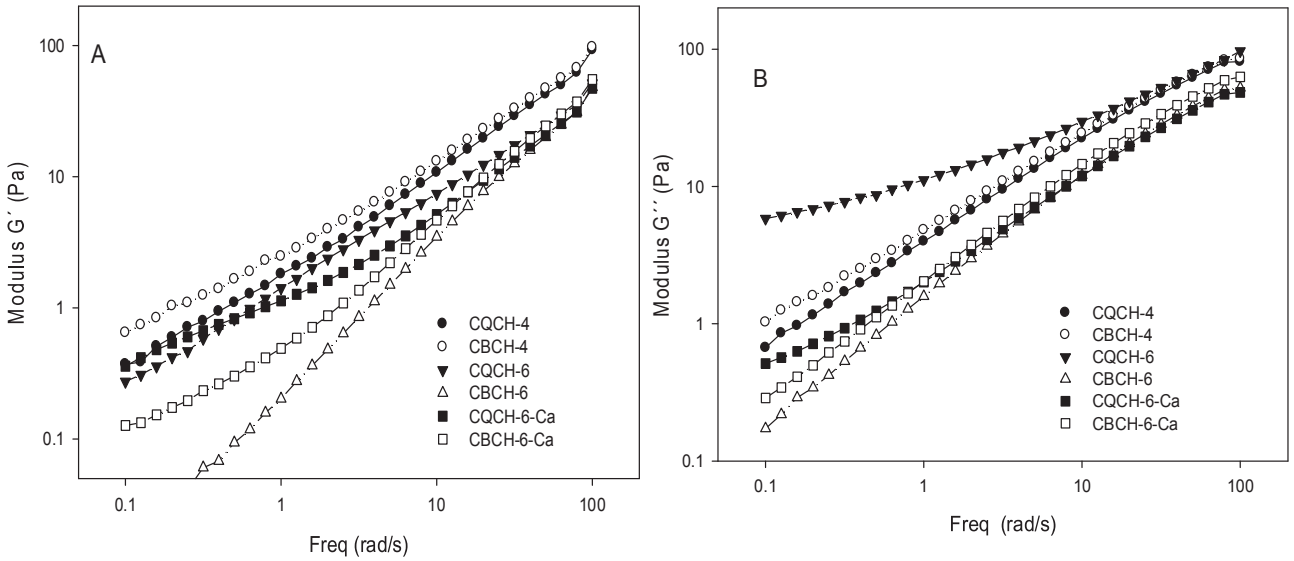

Fig. 3. The dynamic oscillatory behavior of PECs at pH 4, pH 6 with and without Ca^{2+}: A) storage modulus Ǵ and B) loss modulus Ǵ as a function of angular frequency.

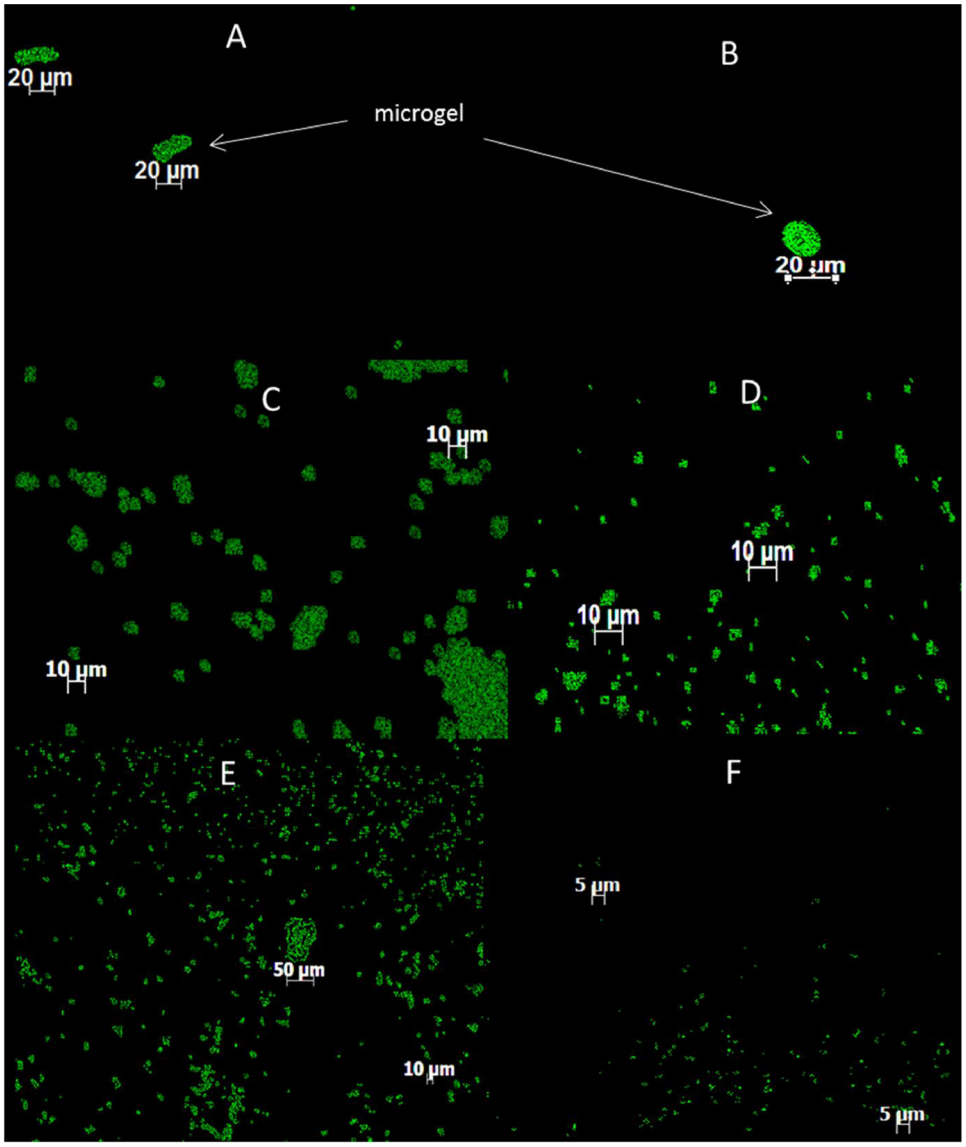

Fig. 4. Images of PECs labeled with CWR and observed in fluorescence microscopy (10x), excitation and emission wavelengths, 370 and 440 nm, respectively: A) CQCH-4, B) CBCH-4; C) CQCH-6; D) CBCH-6; E) CQCH-6-Ca; F) CBCH-6-Ca.

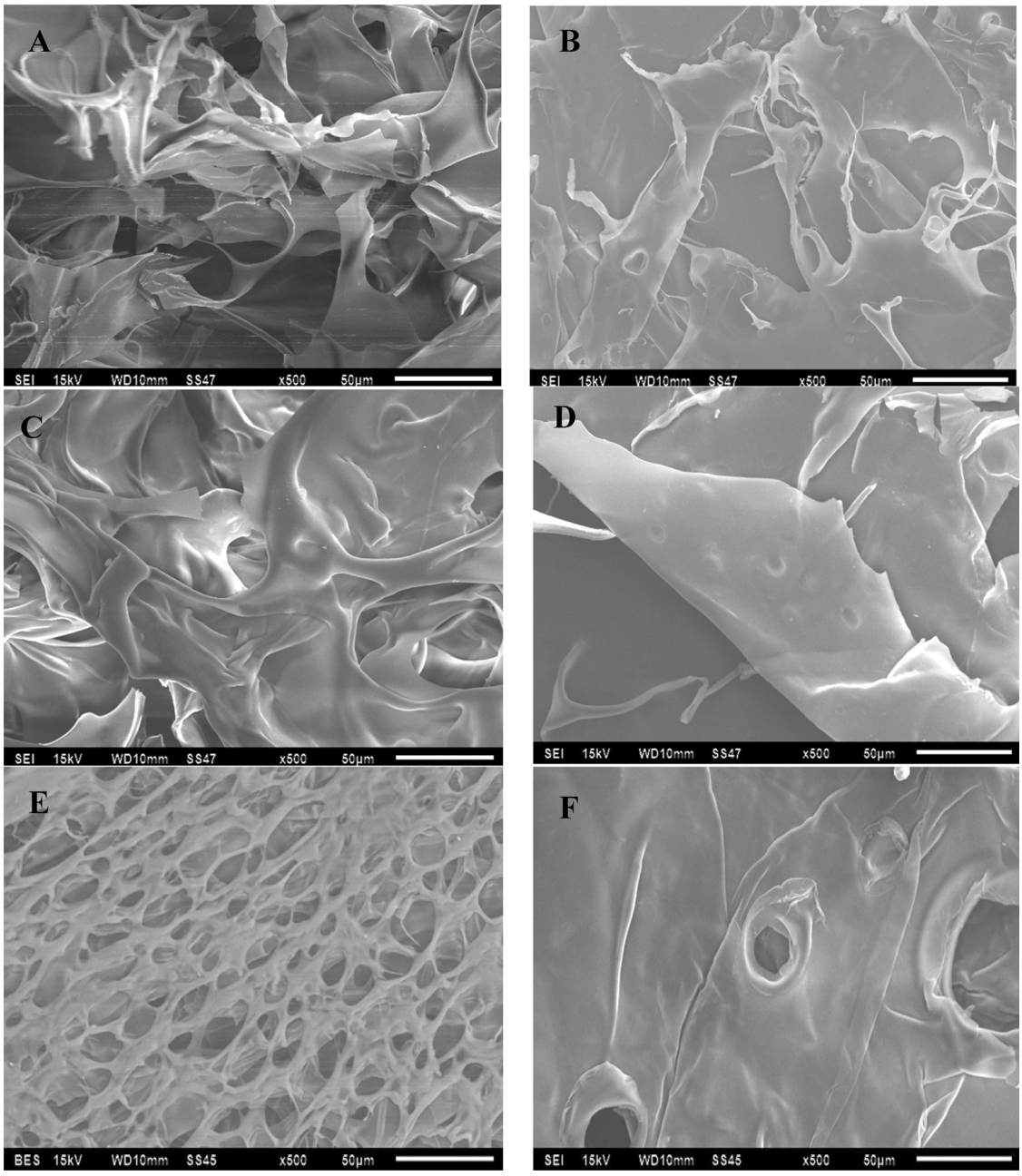

Fig. 5. SEM micrographs of PECs: A) CQCH-4, B) CBCH-4, C) CQCH-6, D) CBCH-6, E) CQCH-6-Ca, F) CBCH-6-Ca.

reported as crosslinked hydrogel particles of small dimension, characterized by its high water content, biocompatibility, and adjustable chemical and mechanical properties (Zhang et al., 2015). Microgels of carboxymethyl cellulose crosslinked to sodium trimetaphosphate and lysozyme were observed with the fluorescence signal from fluorescein isothiocyanate-labeled lysozyme with particle size ranged from 10 to 20 µm (Zhang et al., 2015). The present work displays irregular microgel particles at pH 4 with average diameters of 42.4 µm and 12.8 µm for CQCH-4 and CBCH-4, respectively, whereas at pH 6, a reduction of microgel diameter sizes were observed with 10.8 µm, 18.7 µm and 12.9 µm for CQCH-6, CBCH-6 and CQCH-6-Ca, respectively. The smallest diameter size was 1.5 µm for CBCH-6-Ca; which points out that the DA in BCH might promote a higher interaction than that with QCH, as evidenced by the ζ potential analyses (Fig. 1).

3.3.2. SEM analysis

The SEM of CQCH and CBCH at pH 4 and 6 had no significant differences on APS in a range of 165 and 216 µm (Fig. 5). CQCH and CBCH at pH 4 and pH 6 showed disordered morphology with rough and lamellar structures (Fig. 5A–D). The CBCH with Ca^{+2} ions (Fig. 5F) presented a relatively smooth porous structure, whereas CQCH with Ca^{+2} (Fig. 5E) had a macro rough porous network. Moreover, the structure of the PECs was strongly influenced by the amount of Ca^{+2} ions, thus leading to a more compact, homogeneous and less dense structure than PECs without this cation. The differences in morphology of PECs at pH 6 with and without Ca^{2+} might be due to DA because CQCH-6-Ca had higher DA than CBCH-6-Ca; therefore, the individual interactions with ALG were weaker than those of CBCH resulting in a tridimensional network. Noteworthy, rough surface could be of benefit for cell growth and tissue healing because rougher PECs can adhere to the wounded tissue leading to larger contact surface thereby increasing the contact time (Garrastazu-Pereira et al., 2014).

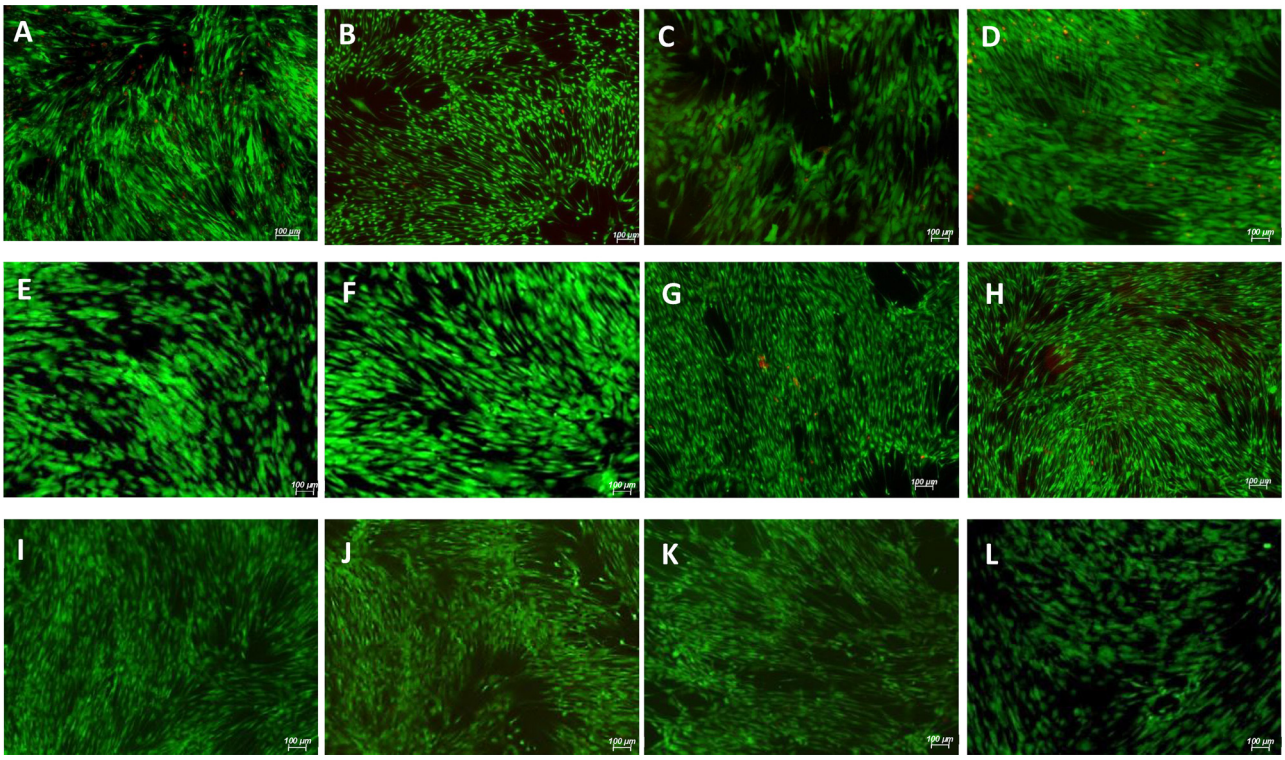

Fig. 6. Fluorescence images of stained HDF with calcein-AM (green) and ethidium homodimer (red). HDFs grew with the following PECs: A) QCH-4, B) BCH-4, C) QCH-6, D) BCH-6, E) QCH-6-Ca, F) BCH-6-Ca, G) CQCH-4, H) CBCH-4, I) CQCH-6, J) CBCH-6, K) CQCH-6-Ca and, L) CBCH-6-Ca. (For interpretation of the references to colour in this figure legend, the reader is referred to the web version of this article.)

3.4. Swelling capacities and degradation studies of the PECs

PECs displayed a fast swelling reaching the equilibrium in 1 h and remained stable up to 24 h (see Supplementary data 5). The CQCH-6 was however an exception reaching the steady state in ca. 24 h, whereas CQCH-4 and CQCH-6-Ca decreased S(%) after this time due to PEC dissolutions. The swelling in PECs might be ascribed to their chemical composition, which contains hydrophilic polysaccharides. Therefore, PECs exhibited considerable swelling (ca. 30-fold) which provides high moisturization, an important feature for wound-dressing interface but also for absorption of any excess of exudate, when not properly removed, can support microbial growth (Pereira et al., 2013).

The degradation profiles of PECs showed that CQCH and CBCH samples at pH 4 and 6 displayed significant differences in weight loss (see Supplementary data 6). PECs at pH 4 had higher weight loss than that at pH 6, which might be due to the acidity that promoted CH dissolution. CQCH-6-Ca degradation was significantly higher than CBCH-6-Ca, which is consistent with the morphology observed by SEM (Fig. 5E). The preservation of molecular weight and crystalline structure of BCH produced materials with low degradation rate regardless the low DA. It can be seen that CQCH-6-Ca presented a network structure with certain porosity at low concentration (1 mM) of Ca^{+2} ions that might favour its rapid dissolution. The use of calcium content higher than 1 mM in the PECs could improve the properties although Lansdown (2002) reported the suppression of proliferation of keratinocytes during the wound healing process with concentration above 1.4 mM. Thus, higher Ca^{2+} concentrations were not attempted.

3.5. Evaluation of cell viability assay and migration of HDF cultured with polysaccharides and PECs

Cells isolated from the dermis layer of foreskin biopsies (HDFs) showed the characteristic fusiform morphology of adhered fibroblasts upon culture, positively expressed characteristic proteins of fibroblasts' ECM, collagen Type I and elastin, and were positive for expression of the fibroblast surface protein (Supplementary data 7). These results corroborated the fibroblastic phenotype of the cells isolated from foreskin biopsies (HDF); cells that were used to study the biological response to the PECs and their components (AV, ALG and CH). Cell viabilities of HDF cultured with the polysaccharides and PECs were studied with the calcein-AM test. The fluorescence images of calcein-AM/ethidium homodimer assays for HDFs cultured showed that their cell viability was negatively impacted by pH, showing a higher percentage of dead cells (over total number of cells) at pH 4 (Fig. 6A,B,G & H) than those at pH 6 (Fig. 6C–G,I–L). The morphology of HDF was also affected at pH 4, losing their characteristic shape, whereas at pH 6 HDFs displayed elongated and fusiform, which is consistent with the statistically significant ($p \leq 0.05$) differences of cell viabilities among CH and PECs at pH 4 and 6. Polysaccharides and PECs with pH 4 were not suitable to promote cell viability, which ranged from 45 to 99%, for polysaccharides at acidic pH cell viability was lower than 30%. Noteworthy, the AV at pH 6 displayed significant positive effects on cell cultures compared to those determined with BCH, QCH and ALG (Supplementary data 8. Images of cell migration in scratch assay of QCH-6, BCH-6, ALG-6 and AV-6). HDFs migration with ALG and AV showed a higher closure of the scratch (wound) than those cultured with QCH-6 and BCH-6. There was also an effect on morphology since HDFs displayed their characteristic fusiform when were cultured with ALG-6 and AV-6, in contrast, cells displayed a more rounded morphology when cultured with QCH-6 and BCH-6. In fact, scratch closure was higher with AV than ALG-6. AV had consistently a positive contribution of cell viability in AV-6-Ca, keeping in mind that this treatment belong to the same group of materials with high cell compatibility and significantly higher than blends of CH/ALG and Ca^{2+}. The effect of AV might be explained by the synergistic action with the AC in agreement with Hamman (2008) who reported enhanced cell proliferation, expression of growth factors involved in skin reparation and production of extracellular matrix (ECM) proteins. The AC is capable of binding to

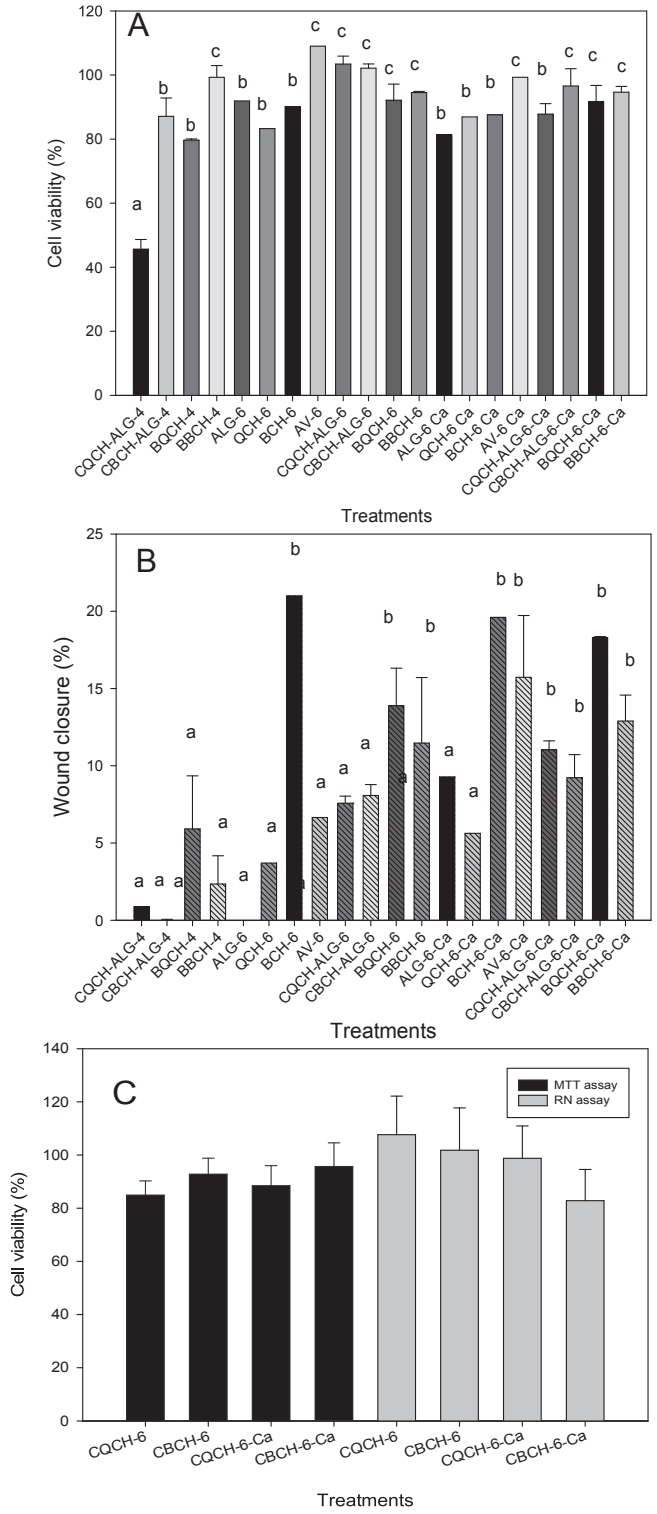

Fig. 7. PECs evaluation on HDFs viabilities (A), percent of wound closure after 24 h of culture (B), HLs viability determined by MTT and NR assays (C). Different letters in histogram mean that the groups are significantly different according to multiple comparisons of means Tukey-Kramer test ($p \leq 0.05$).

mannose receptors in the surface of fibroblasts triggering cell proliferation and growth factors enhancement. Other studies have also demonstrated that AC improves HDFs proliferation by enhanced cyclin D1 protein expression via translational regulation (Thunyakitpisal, Ruangpornvisuti, Kengkwasing, Chokboribal, & Sangvanich 2017). Nevertheless, viability was not significantly different in our samples among cell cultures treated with PECs prepared with either BCH or QCH at pH 6. The PECs at pH 6 with and without Ca^{2+} ions had cell viability greater than 90%, suggesting that these materials and polysaccharides (BCH, QCH, AV or ALG) at pH 6 are biocompatible with HDFs regardless the Ca^{2+} (Fig. 7A).

Fig. 7B shows the percentage of wound closure after culturing with polysaccharides, PECs at pH 4 or 6 with and without Ca^{2+} ions. Additionally, the wound closure of cell cultures with polysaccharides (CH, ALG or AV) at pH 6 is also evidenced. The CBCH-ALG and CQCH-ALG at pH 4, including polysaccharides, exhibited lower wound closure and even negative values than those at pH 6, due to pH damage to the cells. In conclusion, AV combined with Ca^{2+} produced a positive significant effect on HDFs migration. A plausible explanation for these results is the regulation at gene and protein expression levels of basic fibroblasts and transforming β1 growth factors, which are related to wound healing (Hormozi, Assaei, & Beigi Boroujeni, 2017). On the other hand, the PECs with added calcium also presented significant differences enhancement on wound closure. In this regard, Lansdown (2002) reported that Ca^{2+} is involved in epidermis reconstruction owing to its ability of modulation of cell proliferation, motility and maturation. Furthermore, CH could also have a positive effect on cell migration due to the presence of the N-acetyl-D-glucosamine units, the main glycosaminoglycan present in the ECM (Frantz, Stewart, & Weaver, 2010). In the present study, the wound closure (%) was significantly higher for BCH-6 than QCH-6, this might be explained by lower DA in BCH than QCH, which could enhance the HDFs migration as a result of CH degradation in chitooligomers with low DA (Minagawa, Okamura, Shigemasa, Minami, & Okamoto, 2007). However, this effect was not significant on cell migration ($p \leq 0.05$) with PECs added with Ca^{2+} ions (Supplementary data 9. Images of cell migration in scratch assay).

3.5.1. HLs viability

The cell viability was also evaluated by culture of HLs upon incubation with the PECs because these are cellular components of peripheral blood, which interact cell to cell as immune response. HLs are employed in immunotherapy as immunological adjuvants against antigens on the tumor surface like prostate cancer cells (Florczyk et al., 2012). The AC has been reported to enhance cytokine release, activate macrophages and stimulate interaction among them and lymphocytes (Simões et al., 2012). Fig. 7C presents the percentage of cell viability of HLs determined with MTT assay, which was up to 80% without significant difference among PECs prepared at pH 6 ($p > 0.05$). Therefore, there was no evidence of mitochondrial damage as only active mitochondria cleaved the tetrazolium ring of MTT reagent. Additionally, there were no significant differences of HLs viabilities among materials according to NR assay ($p > 0.05$). This substantiated that cell lysosomes kept their integrity and bound to the NR dye. The successful survival of HLs when cultured with PECs might be explained by the release of components with chemical resemblance to the polysaccharides of the ECM, such as glycosaminoglycan (Frantz et al., 2010).

4. Conclusions

PECs composed of CH, AV and ALG have been successfully prepared and characterized for potential application in wound healing. The PECs with entrapped active components of AV offer advantages in the wound healing process such as stability, morphology, water absorption, pore size and rigidity. CQCH-6, CBCH-6 and CQCH-6-Ca and CBCH-6-Ca samples produce a high percentage of HDFs viablity. Remarkably, the AV blended with PECs had a positive effect on cell viability and migration. The PECs prepared at pH 4 presented best physicochemical properties notwithstanding significant reductions on HDFs and HLs viabilities. Importantly, none of these PECs displayed cytotoxicity to HLs confirming their biocompatibility and only CQCH-6-Ca presented some diminution on cell viability.

Acknowledgments

The authors would like to thank Consejo Nacional de Ciencia y Tecnología (CONACyT) for funding Project No. 237292 and scholarship grant (RGR). The authors also thank B. Eng. Mariana Ramírez-Gilly for rheometry analyses and Ana Brena-Molina from the Instituto Nacional de Rehabilitación-LGII for the HDF immunofluorescence assays.

Appendix A. Supplementary data

Supplementary data associated with this article can be found, in the online version, at https://doi.org/10.1016/j.carbpol.2018.03.044.

References

Abduo, E., Nagy, K., & Elsabee, M. (2008). Extraction and characterization of chitin and chitosan from local sources. *Bioresource Technology, 99*(5), 1359–1367. http://dx.doi.org/10.1016/j.biortech.2007.01.051.

Abreu, F., Bianchini, C., Forte, M., & Kist, T. (2008). Influence of the composition and preparation method on the morphology and swelling behavior of alginate–chitosan hydrogels. *Carbohydrate Polymers, 74*(2), 283–289. http://dx.doi.org/10.1016/j.carbpol.2008.02.017.

Annabi, N., Nichol, J. W., Zhong, X., Ji, C., Koshy, S., Khademhosseini, A., et al. (2010). Controlling the porosity and microarchitecture of hydrogels for tissue engineering. *Tissue Engineering: Part B, 16*(4), 371–383. http://dx.doi.org/10.1089/ten.teb.2009.0639.

Berger, J., Reist, M., Mayer, J., Felt, O., Peppas, N., & Gurny, R. (2004). Review: Structure and interactions in covalently and ionically crosslinked chitosan hydrogels for biomedical applications. *European Journal of Pharmaceutics and Biopharmaceutics, 57*(1), 19–34. http://dx.doi.org/10.1016/s0939-6411(03)00160-7.

Bozzi, A., Perrin, C., Austin, S., & Arce Vera, F. (2007). Quality and authenticity of commercial aloe vera gel powders. *Food Chemistry, 103*(1), 22–30. http://dx.doi.org/10.1016/j.foodchem.2006.05.061.

Bunse, S., Garg, S., Junek, S., Vogel, D., Ansari, N., Stelzer, E., et al. (2013). Role of N-cadherin *cis* and *trans* interfaces in the dynamics of adherens junctions in living cells. *PLoS One, 8*(12), 1–16. http://dx.doi.org/10.1371/journal.pone.0081517.

Chang, X., Chen, B., & Feng, Y. (2011). Water-soluble polysaccharides isolated from skin juice, gel juice and flower of *Aloe vera* Miller. *Journal of the Taiwan Institute of Chemical Engineers, 42*(2), 197–203. http://dx.doi.org/10.1016/j.jtice.2010.07.007.

Chokboribal, J., Tachaboonyakiat, W., Sangvanich, P., Ruangpornvisuti, V., Jettanacheawchankit, S., & Thunyakitpisal, P. (2015). Deacetylation affects the physical properties and bioactivity of acemannan, an extracted polysaccharide from Aloe vera. *Carbohydrate Polymers, 133*(1), 556–566. http://dx.doi.org/10.1016/j.carbpol.2015.07.039.

Dao-Thi, M. H., Hamelryck, T. W., Poortmans, F., Voelker, T. A., Chrispeels, M. J., & Wyns, L. (1996). Crystallization of glycosylated and nonglycosylated phytohemagglutinin-L. *Proteins Structure, Function, and Genetics, 24*, 134–137. http://dx.doi.org/10.1002/(SICI)1097-0134(199601)24:1<134:AID-PROT9>3.0.CO ;2-K.

Escobedo-Lozano, A. Y., Domard, A., Velázquez, C. A., Goycoolea, F. M., & Argüelles-Monal, W. M. (2015). Physical properties and antibacterial activity of chitosan/acemannan mixed systems. *Carbohydrate Polymers, 115*(1), 707–714. http://dx.doi.org/10.1016/j.carbpol.2014.07.064.

Florczyk, S. J., Liu, G., Kievit, F. M., Lewis, A. L., Wu, J. D., & Zhang, M. (2012). 3D porous chitosan-alginate scaffolds: New matrix for studying prostate cancer cell-lymphocyte interactions in vitro. *Advanced Healthcare Materials, 1*(5), 590–599. http://dx.doi.org/10.1002/adhm.201100054.

Frantz, C., Stewart, K., & Weaver, V. (2010). The extracellular matrix at a glance. *Journal of Cell Science, 123*(24), 4195–4200. http://dx.doi.org/10.1242/jcs.023820.

Gåserød, O., Smidsrød, O., & Skjåk-Bræk, G. (1998). Microcapsules of alginate-chitosan-I. A quantitative study of the interaction between alginate and chitosan. *Biomaterials, 19*(20), 1815–1825. http://dx.doi.org/10.1016/S0142-9612(98)00073-8.

Garrastazu-Pereira, G., Santos-Oliveira, R., Albernaz, M. S., Canema, D., Weismüller, G., Bede Barros, E., et al. (2014). Microparticles of *Aloe vera*/vitamin E/chitosan: Microscopic, a nuclear imaging and an in vivo test analysis for burn treatment. *European Journal of Pharmaceutics and Biopharmaceutics, 86*(2), 292–300. http://dx.doi.org/10.1016/j.ejpb.2013.10.011.

Gebäck, T., Schulz, M., Koumoutsakos, P., & Detmar, M. (2009). Tscratch: A novel and simple software tool for automated analysis of monolayer wound healing assays. *Biotechniques, 46*(4), 265–274. http://dx.doi.org/10.2144/000113083.

Hamman, J. (2008). Review: composition and applications of *Aloe vera* leaf gel. *Molecules, 13*, 1599–1616. http://dx.doi.org/10.3390/molecules13081599.

Hormozi, M., Assaei, R., & Beigi Boroujeni, M. (2017). The effect of aloe vera on the expression of wound healing factors (TGFβ1 and bFGF) in mouse embryonic fibroblast cell: In vitro study. *Biomedicine & Pharmacotherapy, 88*, 610–616. http://dx.doi.org/10.1016/j.biopha.2017.01.095.

Kačuráková, M., Capek, P., Sasinková, V., Wellnerb, N., & Ebringerová, A. (2000). FT-IR study of plant cell wall model compounds: Pectic polysaccharides and hemicelluloses. *Carbohydrate Polymers, 43*(2), 195–203. http://dx.doi.org/10.1016/S0144-8617(00)00151-X.

Lansdown, A. (2002). Calcium: A potential central regulator in wound healing in the skin. *Wound Repair and Regeneration, 10*(5), 271–285. http://dx.doi.org/10.1046/j.1524-475X.;1;2002.10502.x.

Lawrie, G., Keen, I., Drew, B., Chandler-Temple, A., Rintoul, L., Fredericks, P., et al. (2007). Interactions between alginate and chitosan biopolymers characterized using FTIR and XPS. *Biomacromolecules, 8*(8), 2533–2541. http://dx.doi.org/10.1021/bm070014y.

Lien, S. M., Ko, L. Y., & Huang, T. J. (2009). Effect of pore size on ECM secretion and cell growth in gelatin scaffold for articular cartilage tissue engineering. *Acta Biomaterialia, 5*(2), 670–679. http://dx.doi.org/10.1016/j.actbio.2008.09.020.

Minagawa, T., Okamura, Y., Shigemasa, Y., Minami, S., & Okamoto, Y. (2007). Effects of molecular weight and deacetylation degree of chitin/chitosan on wound healing. *Carbohydrate Polymers, 67*(4), 640–644. http://dx.doi.org/10.1016/j.carbpol.2006.07.007.

Ni, Y., Turner, D., Yates, K. M., & Tizard, I. (2004). Isolation and characterization of structural components of *Aloe vera* L. leaf pulp. *International Immunopharmacology, 4*(14), 1745–1755. http://dx.doi.org/10.1016/j.intimp.2004.07.006.

Pacheco, N., Garnica-González, M., Gimeno, M., Barzana, E., Trombotto, S., David, L., et al. (2011). Structural characterization of chitin and chitosan obtained by biological and chemical methods. *Biomacromolecules, 12*(9), 3285–3290. http://dx.doi.org/10.1021/bm200750t.

Panneerselvam, J., Merlin, R., Kalaivani, T., Baran, M., & Rose, C. (2013). Preparation and characterization of *Aloe vera* blended collagen-Chitosan composite scaffold for tissue engineering applications. *ACS Applied Materials & Interfaces, 5*(15), 7291–7298. http://dx.doi.org/10.1021/am401637c.

Paszek, M. J., Zahir, N., Johnson, K. R., Lakins, J. N., Rozenberg, G. I., Gefen, A., et al. (2005). Tensional homeostasis and the malignant phenotype. *Cancer Cell, 8*(3), 241–254. http://dx.doi.org/10.1016/j.ccr.2005.08.010.

Pereira, R. F., Carvalho, A., Gil, M., Mendes, A., & Bártolo, P. (2013). Influence of *Aloe vera* on water absorption and enzymatic in vitro degradation of alginate hydrogel films. *Carbohydrate Polymers, 98*(1), 311–320. http://dx.doi.org/10.1016/j.carbpol.2013.05.076.

Repetto, G., Del Peso, A., & Zurita, J. (2008). Neutral red uptake assay for the estimation of cell viability/cytotoxicity. *Nature Protocols, 3*(7), 1125–1131. http://dx.doi.org/10.1038/nprot.2008.75.

Sæther, H. V., Holme, H. K., Maurstad, G., Smidrød, O., & Stokke, B. T. (2008). Polyelectrolyte complex formation using alginate and chitosan. *Carbohydrate Polymers, 74*(4), 813–821. http://dx.doi.org/10.1016/j.carbpol.2008.04.048.

Schneider, C. A., Rasband, W. S., & Eliceiri, K. W. (2012). NIH Image to ImageJ: 25 years of image analysis. *Nature Methods, 9*(7), 671–675. http://dx.doi.org/10.1038/nmeth.2089.

Silva, S., Caridade, S., Mano, J., & Reis, R. (2013). Effect of crosslinking in chitosan/*Aloe vera*-based membranes for biomedical applications. *Carbohydrate Polymers, 98*(1), 581–588. http://dx.doi.org/10.1016/j.carbpol.2013.06.022.

Silva, S., Popa, E., Gomes, M., Cerqueira, M., Marques, A., Caridade, S., et al. (2013). An investigation of the potential application of chitosan/aloe-based membranes for regenerative medicine. *Acta Biomaterialia, 9*(6), 6790–6797. http://dx.doi.org/10.1016/j.actbio.2013.02.027.

Simó, G., Fernández-Fernández, E., Vila-Crespo, J., Ruipérez, V., & Rodríguez-Nogales, J. M. (2017). Research progress in coating techniques of alginate gel polymer for cell encapsulation. *Carbohydrate Polymers, 170*(15), 1–14. http://dx.doi.org/10.1016/j.carbpol.2017.04.013.

Simões, J., Nunes, F. M., Domingues, P., Coimbra, M. A., & Domingues, M. R. (2012). Mass spectrometry characterization of an Aloe vera mannan presenting immunostimulatory activity. *Carbohydrate Polymers, 90*(1), 229–236. http://dx.doi.org/10.1016/j.carbpol.2012.05.029.

Thunyakitpisal, P., Ruangpornvisuti, V., Kengkwasing, P., Chokboribal, J., & Sangvanich, P. (2017). Acemannan increases NF-κB/DNA binding and IL-6/-8 expression by selectively binding toll-like receptor-5 in human gingival fibroblasts. *Carbohydrate Polymers, 161*, 149–157. http://dx.doi.org/10.1016/j.carbpol.2016.12.034.

Velasquillo, C., Silva-Bermudez, P., Vázquez, N., Martínez, A., Espadín, A., García-López, J., et al. (2017). In vitro and in vivo assessment of lactic acid-modified chitosan scaffolds for potential treatment of full-thickness burns. *Journal of Biomedical Materials Research Part A, 105A*, 2875–2891. http://dx.doi.org/10.1002/jbm.a.36132.

Yang, Y., Campanella, O., Hamaker, B., Zhang, G., & Gu, Z. (2013). Rheological investigation of alginate chain interactions induced by concentrating calcium cations. *Food Hydrocolloids, 30*(1), 26–32. http://dx.doi.org/10.1016/j.foodhyd.2012.04.006.

Zhang, B., Sun, B., Li, X., Yu, Y., Tian, Y., Xu, X., et al. (2015). Synthesis of pH- and ionic strength-responsive microgels and their interactions with lysozyme. *International Journal of Biological Macromolecules, 79*, 392–397. http://dx.doi.org/10.1016/j.ijbiomac.2015.05.011.